J Solid State Electrochem (2012) 16:1161–1168
DOI 10.1007/s10008-011-1489-2

ORIGINAL PAPER

The effect of loading and particle size on the oxygen reaction in CGO impregnated Pt electrodes

Anders Lund · Karin Vels Hansen · Torben Jacobsen · Mogens Mogensen

Received: 10 December 2010 / Revised: 18 June 2011 / Accepted: 26 June 2011 / Published online: 23 July 2011

Abstract Porous platinum electrodes impregnated with $Gd_xCe_{1-x}O_{2-\delta}$ (CGO) are investigated to characterise how nano-sized CGO grains affect the oxygen reaction. Impedance measurements were performed at temperatures between 450 and 750 °C and at oxygen partial pressures of 0.2 and 5×10^{-5} bar for electrodes with various CGO loadings and electrodes annealed at various temperatures. The morphology was characterised by scanning electron microscopy and the CGO grain size was determined from X-ray diffraction peak broadening. The results showed that the polarisation resistance decreased with increasing CGO loading and increasing annealing temperature. CGO facilitates transport of oxygen ions thereby increasing the effective triple-phase boundary.

Keywords Impregnation · Electrode · Impedance · Oxygen · Platinum

Introduction

In solid-state gas sensor electrodes, the electrochemical reactions are confined to regions close to the boundary between the electronic and the ionic conducting phases and the gas phase, the so called triple-phase boundary (TPB). Due to this limitation of the active area, the reactivity is very sensitive to impurities like silicates segregating from the ceramic electrolyte. The influence of impurities might be reduced by increasing the TPB length through impregnation of porous platinum with ionically conducting materials like gadolinia doped ceria (CGO). Gadolinium (III) oxide doping of cerium(IV) oxide induces formation of oxygen vacancies and thereby high ionic conductivity [1, 2]. The ionic conductivity of nanocrystalline CGO increases with decreasing grain size, going from 36 to 11 nm, but it does not exceed the bulk conductivity of micron-sized crystals [3].Therefore, both the gadolinium (III) oxide doping and the decreasing crystal size may improve the electrochemical properties. Nano-sized CGO particles can be produced by impregnation and are used in catalysts because of their ability to release or absorb oxygen quickly [4, 5]. However, there are only few investigations of the effect of impregnation with CGO on the oxygen reaction in electrodes [6–8]. The incorporation of ionically conducting metal oxides in Pt cermet electrodes has previously been shown to decrease the activation energy of the charge transfer process and improve the catalytic properties [9–11].

Platinum is the most commonly used material for oxygen sensor electrodes because of its good electrocatalytic properties and stability [12–15]. The catalytic activity of platinum is reduced heavily below 500 °C and therefore sensors with platinum electrodes are normally operated around 700 °C [16]. Important parameters for the practical application of oxygen sensors are the response time and the sensitivity in particular at low oxygen partial pressures. If the oxygen reaction is too slow it may lead to erroneous measurements. Impurities and the formation of

Electronic supplementary material The online version of this article (doi:10.1007/s10008-011-1489-2) contains supplementary material, which is available to authorized users.

A. Lund (✉) · T. Jacobsen
Department of Chemistry, Technical University of Denmark,
DK-2800 Kongens Lyngby, Denmark
e-mail: andlund@gmail.com

K. V. Hansen · M. Mogensen
Fuel Cells and Solid State Chemistry Division,
Risø National Laboratory for Sustainable, Energy,
Technical University of Denmark,
DK-4000 Roskilde, Denmark

oxide layers on platinum may reduce the active triple-phase boundary (TPB) length and slow down the oxygen reaction.

The present paper explores the effect of CGO on the electrochemical properties of porous platinum electrodes on yttria-stabilised zirconia (YSZ) electrolytes by impedance spectroscopy. The main focus is to resolve which processes are dominating the electrode impedance for various CGO loadings and CGO grain sizes. The measurements were performed at various temperatures and oxygen partial pressures.

Experimental

Dense 4×4-cm^2-large and 200-μm-thick 8-mol% YSZ tapes were painted with a Bi-containing platinum paste (Engelhard, No: 6082A) four times on each side and sintered in air at 900 °C to produce two identical 4×4-cm^2-large and 10±5 μm thick porous electrodes. These tapes were then cut into 0.5×0.5 cm^2 planar cells with two identical porous platinum electrodes. Some of the platinum electrodes were impregnated with a solution of cerium(IV)nitrate (99.5%, Alfa Aesar) and gadolinium(III)nitrate (99.9%, Alfa Aesar) containing deionised water. Pluronic 123 (P123, BASF) was used as a surfactant and either 2.5 or 10 wt.% was added to the solution. Solutions corresponding to two different compositions, $Ce_{0.8}Gd_{0.2}O_{2-\delta}$ (CGO20) and $Ce_{0.9}Gd_{0.1}O_{2-\delta}$ (CGO10), were produced. The impregnated electrodes were dried and excess P123 and nitrates was gently removed with a paper towel. Nano-sized CGO particles were formed by calcining the electrode at 300 °C in flowing air. The CGO loading was calculated as $c_A=m_{CGO}/2A$, where A is the area of the cell (with two electrodes) and m_{CGO} is the mass of CGO. Table 1 lists the electrodes investigated in this paper. Prior to measurements, the impregnated electrodes were annealed for 12–24 h to obtain a stable grain size [17]. The series of electrodes 4.2 to 4.9 were annealed at temperatures between 550 and 750 °C to produce CGO of different grain sizes. The series of impregnated electrodes 3.5 to 3.9 and 4.19 to 4.23 were annealed at 750 and 706 °C, respectively, to obtain similar grain sizes and different CGO loadings.

The formation of the CGO fluorite structure was verified by X-ray diffraction (XRD) using a Bruker D8 Advance diffractometer and using the Cu K_α radiation. The mean grain size, d, was calculated by applying the Scherrer method to the (111) line of CGO at 2θ=29° [18]. The relation $d=K\lambda/\beta\cos(\theta)$ was used. The shape factor, K, was assumed to be 0.9, θ is the scattering angle, λ=0.154 nm is the X-ray wavelength and β is the full width at half maximum. The instrumental broadening was $2\theta\approx0.05°$. The platinum grains are too large for the size to be determined from XRD peak broadening.

For each electrochemical test up to four cells were placed in a furnace with an inlet gas flow of 6.0 L/h. The temperature of the furnace was controlled with an accuracy of ±1 °C The oxygen partial pressure was determined by a potentiometric oxygen sensor positioned next to the cells. Each cell was placed between two alumina blocks with a platinum mesh and pressed together by a load to ensure good electrical contact. The impedance of the series of electrodes 4.19 to 4.23 was measured in flowing air at 706 °C. The impedance of the series of electrodes 3.5 to 3.9 was measured between 500 and 750 °C in flowing air. The impedance of the electrodes 4.2 to 4.9 was measured between 443 °C and the annealing temperature, T_A, in flowing N_2 with oxygen partial pressures

Table 1 List of electrodes investigated. c_A is the loading, N_I is the number of impregnations, c_M is the molar concentration of the cations, T_A is the annealing temperature, w_{P123} is the wt.% of P123 in solution, β is the full width at half maximum of the XRD line and d is the grain size obtained from the XRD peak broadening

Cells	$c_A/\frac{mg}{cm^2}$	N_I/	$c_M/\frac{mole}{L}$	w_{P123}/wt%	T_A/°C	β(111)/	d/nm	
Pt	–	–	–	–	–	–	–	
3.5	(CGO20)	0.46	2	3	10	750	–	–
3.7	(CGO20)	0.54	2	3	10	750	–	–
3.9	(CGO20)	0.63	3	3	10	750	–	–
4.2	(CGO20)	0.51	2	3	10	750	0.42±0.07	20±3
4.5	(CGO20)	0.34	2	3	10	700	0.42±0.04	20±2
4.6	(CGO20)	0.74	2	3	10	650	0.53±0.04	15±1
4.7	(CGO20)	0.65	2	3	10	600	0.55±0.04	15±1
4.9	(CGO20)	0.43	2	3	10	550	0.85±0.08	10±1
4.19	(CGO10)	0.47	2	3.5	2.5	706	–	–
4.20	(CGO10)	0.37	1	2.5	2.5	706	–	–
4.22	(CGO10)	0.17	1	1	2.5	706	–	–
4.23	(CGO10)	0.07	1	0.21	2.5	706	–	–

of around 5×10^{-5} bar. The measurement at the highest temperature was performed first and the measurement at the lowest temperature, last. The measurements were performed at open circuit voltage with an AC root mean square amplitude of 50–100 mV. A Solartron 1260 frequency response analyser was used to conduct the EIS measurements. The cell impedance was analysed with equivalent circuit modelling by nonlinear least square fitting in MatLab applying the Levenberg–Marquardt algorithm and standard errors were calculated using a confidence interval of 95%.

Cells were fractured to investigate the morphology of a cross section. The SEM investigations were performed using field emission SEM (Zeiss SUPRA-35 and Zeiss X-beam 1540) with a secondary electron detector.

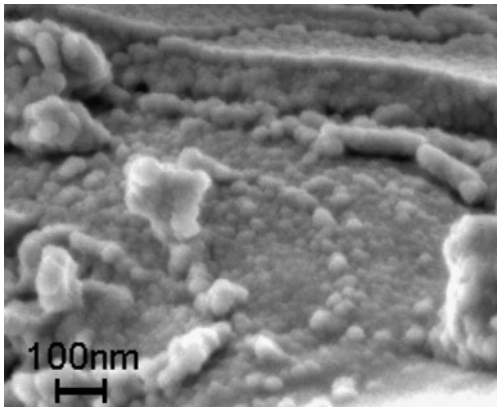

Fig. 2 SEM (SE) image showing agglomerated CGO20 grains on a platinum grain, c_A=0.51 mg cm^{-2} and T_A=750 °C (electrode 4.2)

Results

SEM examination of the impregnated electrode 4.20 showed that most of the CGO10 was found in the pores of the platinum electrode as porous agglomerates and as discrete grains and agglomerates scattered across the platinum surface. Figure 1 shows CGO10 grains and agglomerates on the surface of a platinum grain and in the pores. The pores of the platinum electrode are not completely filled with CGO10. The size of the platinum grains and the pores is 1–2 μm, while the size of the CGO10 grains is less than 30 nm. The electrode, 4.2, in Fig. 2 was impregnated twice using a higher cation and surfactant concentration compared with the impregnated electrode in Fig. 1. CGO20 agglomerates were found both in the pores and as a layer, which was around 200 nm thick, on the platinum surface. The CGO20 grain size is seen to be less than 30 nm which is in agreement with the grain size obtained from XRD peak broadening, Table 1. In both electrodes, the CGO was distributed uniformly throughout the electrode.

EIS measurements in air

Impedance measurements were performed on both CGO10 and CGO20 impregnated electrodes. Fig. 3 shows the Nyquist plots for CGO10 loadings up to 0.47 mg cm^{-2}. The impedance was normalised with the area of the electrode projection on the electrolyte. The measurements were performed in a frequency range from 13 Hz to 32 kHz with between 5 and 15 points per decade. The morphology of the electrodes with high CGO10 loadings, 0.37 mg cm^{-2} and above, was similar to that in Fig. 1. However, for a loading of only 0.07 mg cm^{-2}, the CGO10 was only found as discrete agglomerates. The polarisation resistance decreased with increasing loading of CGO10 until 0.37 mg cm^{-2}. For a higher loading of 0.47 mg cm^{-2}, it was increased. One arc was identified by equivalent circuit modelling for the impregnated and the single-phase platinum electrode. The data were therefore fitted with the model $(R_s)(L)(R_eQ_e)$ (Fig. 3) The equivalent circuit corresponding to the model is shown in Fig. 3. The series resistance, R_s, represents the ohmic loss due to transport of oxide ions in the YSZ electrolyte and it is frequency independent. The inductance,

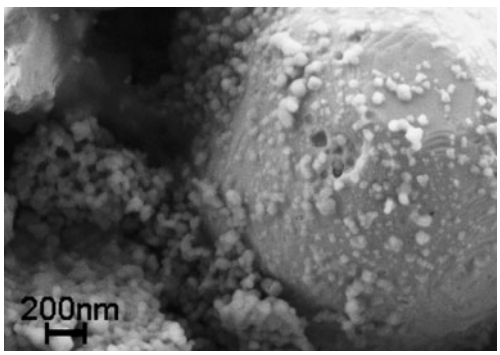

Fig. 1 SEM (SE) image showing CGO10 grains and agglomerates scattered discretely over a platinum grain, c_A=0.37 mg cm^{-2} and T_A=706 °C (electrode 4.20)

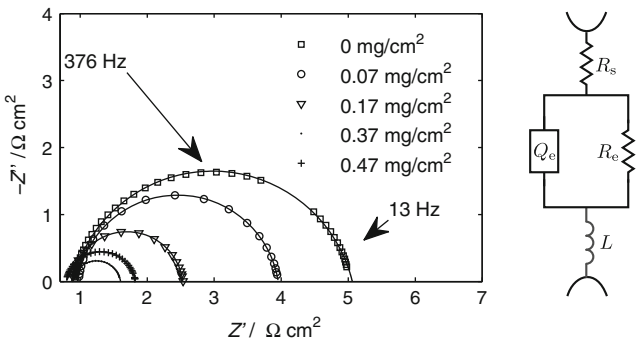

Fig. 3 Nyquist plot with fits for various loadings of CGO10. The measurements were performed at p_{O2}=0.2 bar at 706 °C on a single-phase platinum electrode and the impregnated electrodes 4.19 to 4.23

L, is included to take into account high frequency inductance and instrumental artefacts. The oxygen reaction is represented with an RQ-circuit where R_e is the polarisation resistance and Q_e is the constant phase element. The characteristic frequency of the oxygen reaction was calculated as $2\pi f_e = (R_e Q_e)^{-1/n_e}$ and the apparent capacitance as [19] $C_e = \left(Q_e R_e^{1-n_e}\right)^{1/n_e}$. The admittance of $(R_e Q_e)$ is given by $Y = 1/R_e + Q_e(i\omega)^{n_e}$. If n_e=1, Q_e has the units of a capacitance and $0<n_e<1$ corresponds to a depression of the semicircle in the Nyquist plot.

Table 2 lists the results from fitting of R_e, n_e, the characteristic frequency, f_e, and the apparent capacitance, C_e. The addition of CGO10 resulted in the increase in the polarisation resistance from 3.9 Ω cm^2 for the single-phase platinum electrode to 0.7 Ωcm^2 for the electrode with a loading of 0.37 mg cm^{-2}. The polarisation resistance of two identically prepared platinum electrodes was found to be 3.9 and 4.2 Ωcm^2 confirming that the effect of CGO10 is beyond the experimental error. The addition of CGO10 resulted in an increase in the characteristic frequency from 0.46 kHz for the single-phase platinum electrode to 2.7 kHz for the electrode containing 0.37 mg cm^{-2}. It had only a small effect on the series resistance R_s and the capacitance, C_e, as given by the table values. The exponent n_e was found to be around 0.9 for the impregnated and the single-phase platinum electrode. The capacitance of 88 μFcm^{-2} for the single-phase platinum electrode was slightly higher than 20–70 μF cm^{-2} which has previously been reported for the oxygen reaction at the platinum/YSZ interface [20, 21].

CGO20 impregnated electrodes

Figure 4 shows the normalised Nyquist plot for measurements performed between 500 and 750 °C at an oxygen partial pressure of 0.2 bar on a CGO20 impregnated electrode, 3.5. The impedance was measured in a frequency range from 0.5 Hz to 120 kHz with five to ten points per decade. The morphology of the electrodes were similar to that shown in Fig. 2. The porous layer of CGO on the platinum surface may form a percolating oxide ion conducting phase and the oxygen reaction may therefore be distributed across the platinum surface.

Table 2 Fitted parameter values obtained from measurements at 706 °C at an oxygen partial pressure of 0.2 bar on a single-phase platinum electrode and CGO10 impregnated electrodes, 4.19 to 4.23

c_A/mg cm^{-2}	0	0.07	0.17	0.37	0.47
L/μH	0.06	0.08	0.04	0.02	0.03
R_s/Ω cm^2	1.0	0.96	0.87	0.89	0.79
R_e/Ω cm^2	3.9	3.0	1.7	0.7	1.0
C_e/μF cm^{-2}	88	69	62	82	78
n_e	0.91	0.90	0.93	0.91	0.91
f_e/kHz	0.46	0.79	1.6	2.7	2.0

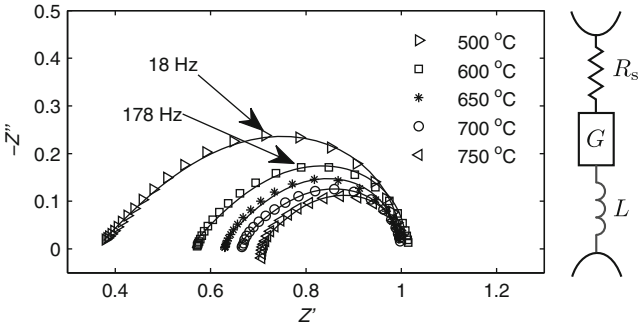

Fig. 4 Normalised Nyquist plot with fits. The measurements were performed at an oxygen partial pressure of 0.2 bar at various temperatures on the CGO20 impregnated electrode 3.5 (0.46 mg cm^{-2}).

A simple way of modelling a distributed oxygen reaction is using a semi-infinite transmission line, Fig. 5 [22]. The ohmic loss due to transport of oxide ions in the CGO phase is represented by a resistor, R_{CGO}. The oxygen reaction is represented by an RQ-circuit, where R_e is the oxygen reaction resistance and Q_e is a constant phase element which represents the apparent capacitance and accounts for the depression of the semi-circles. The impedance of the semi-infinite transmission line is equivalent to that of a Gerischer-type impedance [22].

$$Z_G = \left(\frac{R_{CGO}}{\frac{1}{R_e} + Q_e(iw)^{n_e}}\right)^{1/2} \quad (1)$$

where the DC resistance is given by $(R_{CGO}R_e)^{1/2}$. Hitz and Lasia [23] have also shown that a Gerischer-type impedance may be observed for porous electrodes which have percolating electronic and ionic conductive phases.

The measurements were therefore fitted with the model $(R_s)(L)(G_e)$, where G_e is a Gerischer-type element, which represents the oxygen reaction at the porous electrode. The exponent n_e was constrained to be between 0.9 and 1 to take into account the depression of the arcs. The constant

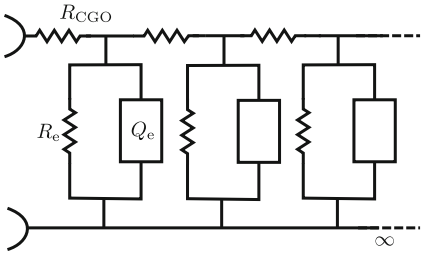

Fig. 5 A semi-infinite transmission line, where R_{CGO}, represents the ionic resistance in the CGO phase and R_e is the oxygen reaction resistance and Q_e is a constant phase element which represents the apparent capacitance of the oxygen reaction

phase element, Q_e, was fixed when fitting using the obtained value of $C_e \approx 80$ μF cm^{-2} from Table 2, to decrease the number of free parameters to 5. Figure 4 shows that the model fits to the impedance. For the electrode 3.5 (0.46 mg cm^{-2}), R_e was found to be 2.5 Ωcm^2 and R_{CGO} was found to be 0.15 Ωcm^2 at 700 °C. The addition of CGO20 resulted in a decrease in the total polarisation resistance $R_p = \sqrt{R_{CGO}R_e}$ from 3.9–4.2 Ωcm^2 for the single-phase platinum electrode to 0.60–0.74 Ωcm^2, as given in Table 3. Furthermore, it increased the characteristic frequency slightly from 0.37–0.48 kHz for the single-phase platinum electrode to 0.39–0.6 kHz.

Figure 6 shows that the polarisation resistance, R_e, decreases with increasing CGO load up to a loading around 0.4 mg cm^{-2}. The increase in the characteristic frequency, f_e, up to around 0.4 mg cm^{-2} reflects the decrease in the polarisation resistance since the capacitance is not changed significantly. The decrease in the characteristic frequency observed at high loadings may on the other hand reflect a change in the reaction mechanism. The impedance of the impregnated electrodes 3.5 to 3.9 was fitted with a Gerischer-type element.

The activation energy of the series resistance, R_s, was found to be 0.7–0.9 eV which is in accordance with the oxide ion conductivity of bulk YSZ [24]. The apparent activation energies of R_e was found to be 1.2–1.5 eV for the impregnated electrodes and it was 2.2±0.3 eV for the single-phase platinum electrode. The activation energy obtained for the single-phase platinum electrode is in agreement with previous results obtained from impedance spectroscopy by Velle and Norby [11]. The activation energy of R_{CGO} was found to be 1.2±0.1 eV for the impregnated electrodes.

EIS measurements in N_2

The series of impregnated electrodes, 4.2 to 4.9 were annealed from 550 to 750 °C to investigate the electrochemical properties as function of the CGO grain size and the annealing temperature. These electrodes were impregnated with CGO20. The CGO loading was between 0.34 and 0.74 mg cm^{-2} and should therefore have little effect on

Table 3 Fitted parameters obtained from measurements performed at 700 °C and an oxygen partial pressure of 0.2 bar on CGO20 impregnated electrodes (3.5-3.9)

c_A/mg cm^{-2}	0.46	0.54	0.63
L/μH	0.02	0.02	0.01
R_s/Ω cm^2	1.1	0.96	0.92
R_p/Ω cm^2	0.60	0.74	0.66
n_e	1.0	1.0	1.0
f_e/kHz	0.69	0.46	0.39

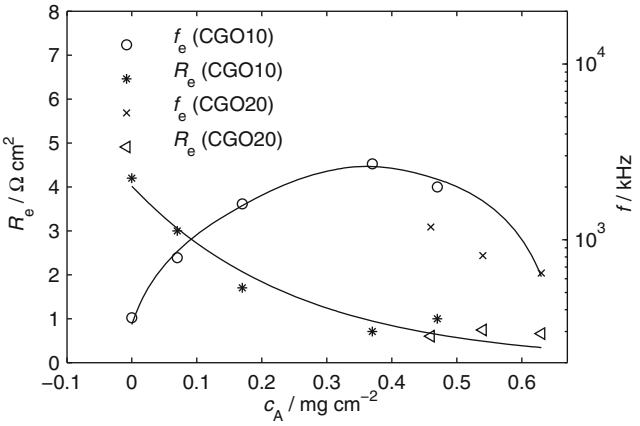

Fig. 6 The characteristic frequency and polarisation resistance as functions of the CGO loading. The measurements were performed at 700 °C (CGO20) and 706 °C (CGO10) at an oxygen partial pressure of 0.2 bar. The polarisation resistance was fitted with an exponential decaying function

the polarisation resistance as described earlier. The morphology of the impregnated electrodes was similar to that observed in Fig. 2. Figure 7 shows an almost linear relationship between the mean grain size, d, obtained from XRD peak broadening and the equilibration temperature, Table 1. The grain size is in agreement with previous results reported by Levy et al. [25]. Impedance spectroscopy measurements were performed at an oxygen partial pressure of around 5×10^{-5} bar between 443 and 744 °C. Figure 7 shows that the polarisation resistance obtained at around 500 °C, decreased with increasing annealing temperature.

Figure 8 shows the Nyquist plot obtained at various temperatures from measurements on the impregnated electrode annealed at 700 °C. The measurements were performed in a frequency range from 90 mHz to 10 kHz. At 494 °C and below, a temperature dependent arc dominates

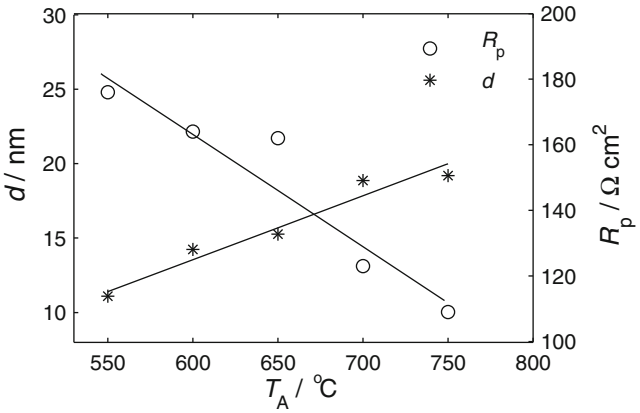

Fig. 7 The mean grain size, d, measured by XRD peak broadening and the electrode polarisation resistance of the impregnated electrodes 4.2 to 4.9 as functions of the annealing temperature for measurements performed at around 500 °C and at an oxygen partial pressure around 5×10^{-5} bar

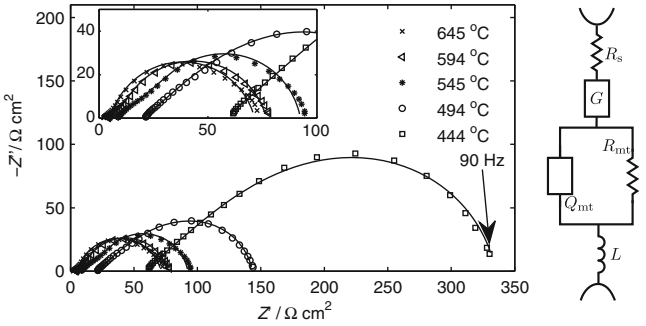

Fig. 8 Nyquist plot obtained for the impregnated electrode, 4.5, at various temperatures and at an oxygen partial pressure of 5×10^{-5} bar

the impedance spectrum. This arc is thought to be related to the oxygen reaction and is represented with a Gerischer-type impedance as mentioned above. Between 594 and 645 °C, a nearly temperature-independent arc dominated the impedance spectrum.

The gas phase mass transport processes, gas diffusion and convection, are nearly temperature independent. Gas diffusion may give rise to an arc in the Nyquist plot and the gas diffusion resistance is given by [26].

$$R_d = \left(\frac{\mathrm{R}T}{2\mathrm{F}}\right)^2 \frac{1}{P\mathrm{D}_{\mathrm{eff}}} \frac{1}{x_{\mathrm{O}_2}} \tag{2}$$

where R is the gas constant, T is the temperature, F is the Faraday constant, P is the pressure, D_{eff} is the effective diffusion coefficient and x_{O_2} is the molar fraction of oxygen. Gas conversion impedance may be represented with an RC-circuit, R_cC_c, using the continuously stirred tank reactor model [27, 28].

The polarisation resistance is given by

$$R_{\mathrm{c}} = \frac{\mathrm{R}T}{16\mathrm{F}^2 J_{\mathrm{i}}} \frac{1}{x_{\mathrm{i,O}_2}} \tag{3}$$

where J_i is the inlet gas flow and $x_{\mathrm{i,O}_2}$ is the molar fraction of oxygen in the inlet gas. With an inlet gas flow of 6.0 L/h at 744 °C at an oxygen partial pressure of 5×10^{-5} bar, the gas conversion resistance was calculated to be 4.8 $\Omega\mathrm{cm}^2$. The gas phase mass transport processes are probably related to gas convection and diffusion and were represented by an RQ-circuit, ($R_{\mathrm{mt}}Q_{\mathrm{mt}}$). The exponent n_{mt} was used to take into account the depression of the arc in the Nyquist plot. The impedance of the single-phase platinum electrode was therefore fitted with the model $(R_s)(L)(R_eQ_e)(R_{mt}Q_{mt})$ and that of the impregnated electrodes was fitted with the model $(R_s)(L)(G)(R_{mt}Q_{mt})$. At 744 °C, the addition of CGO20 resulted in a decrease in the polarisation resistance from 62 $\Omega\mathrm{cm}^2$ for the single-phase platinum electrode to 34 $\Omega\mathrm{cm}^2$ for the electrode annealed at 750 °C. R_{mt} was found to be 33 and 32 $\Omega\mathrm{cm}^2$ for the single-phase platinum and the impregnated electrode, respectively. The characteristic frequency of the mass transport processes was found to be f_{mt}= 2 and 4 Hz for the impregnated and the single-phase platinum electrode, respectively, and the exponent n_{mt} was found to be between 0.9 and 1.0 for all the electrodes.

At around 500 °C, the addition of CGO20 resulted in a decrease in the polarisation resistance from 656 $\Omega\mathrm{cm}^2$ for the single-phase platinum electrode to 109 $\Omega\mathrm{cm}^2$ for the impregnated electrode annealed at 750 °C (Table 4).

The addition of CGO20 resulted in a decrease in the characteristic frequency according to Table 4. The characteristic frequency of the impregnated electrodes decreased with increasing annealing temperature.

The apparent activation energy of R_e was found to be 1.0± 0.1 eV for the single-phase platinum electrode and 1.5–1.6 eV for the impregnated electrodes. The activation energy of R_{CGO} was found to be 0.7–0.9 eV.

Discussion

The difference in the CGO coverage of the platinum surface between the two electrodes shown is probably related to the concentration of surfactant used in the solution. The electrode with the high coverage was impregnated with a solution containing four times the amount of surfactant compared with the electrode having a low coverage.

The oxide ion conductivity of nano-sized CGO20 grains is almost twice that of CGO10 [3], and this may affect the electrochemical properties. However, a process related to the transport of oxide ions in the CGO phase was only observed for the CGO20 impregnated electrodes and therefore it is not possible to determine the effect of the difference in ionic conductivity between CGO10 and CGO20.

The addition of even a small amount of CGO decreased the polarisation resistance possibly by increasing the TPB length and/or the catalytic activity. The decrease in the polarisation resistance, R_e, with increasing loading showed that there was a loading for which there is no further improvement, around 0.4 mg cm^{-2}. Beyond this, the extra CGO had no significant effect on the polarisation resistance. For small loadings, CGO did not affect the capacitance of the Pt/YSZ interface significantly, and it

Table 4 Fitted parameters obtained at around 500 °C and at an oxygen partial pressure of around 5×10^{-5} bar on the impregnated electrodes, 4.2 to 4.9

T_A/°C	Pt	750	700	650	600	550
L/μH	60	31	3	55	85	22
R_s/Ω cm²	17	22	17	19	17	19
R_p/Ω cm²	656	109	123	162	164	176
n_e	0.90	0.91	0.90	0.90	0.94	0.91
f_e/Hz	3.1	2.9	2.3	2.2	2.1	2.1

was found to be around 80 μF cm^{-2} (Table 2). The impedance spectrum was changed for the impregnated electrodes with a high loading and when the CGO formed a layer on the platinum surface.

The impedance was fitted with a Gerischer-type impedance and in this model it was assumed that oxide ions are transported in the CGO phase as illustrated in Fig. 9. Oxygen may therefore react at the Pt/CGO interface which increases the effective TPB length. The oxygen probably reacts near the Pt/YSZ TPB and therefore a saturation is observed when the extra CGO is deposited outside this region.

Silicate impurities segregate to the surface during high temperature sintering [29, 30] and are known to inhibit the electrochemical properties of the platinum electrode by blocking the oxygen reaction [31]. If the impurities are deposited at the TPB, as shown in Fig. 9, they block the oxygen reaction. Impurities might segregate to the CGO grains thereby cleaning the TPB at the Pt/YSZ interface. Due to the high specific surface area of the CGO grains, the effect might be significant. This may explain the decrease in the polarisation resistance and the increase in the characteristic frequency for small loadings, <0.4 mg cm^{-2}. But for higher loadings the transport of oxide ions in the CGO phase was observed to affect the electrochemical properties, as mentioned above.

The impedance obtained from measurements on the electrodes with a high loading were fitted with a Gerischer-type impedance as mentioned above. The apparent activation energy of 1.2±0.1 eV for R_{CGO} corresponds to transport of oxide ions in CGO [3]. The apparent activation energy of the oxygen reaction, R_e, was lowered from 2.2 eV for the single-phase platinum electrode to 1.2–1.5 eV for the impregnated electrodes, for measurements performed at an oxygen partial pressure of 0.2 bar. The decrease in the apparent activation energy indicated that the oxygen reaction is catalysed by CGO. At low oxygen partial pressures, around 5×10^{-5} bar, CGO increased the apparent activation energy from 1 eV for the single-phase platinum electrode to 1.5–1.6 eV for the impregnated electrodes. However, CGO reduced the polarisation resistance in the temperature range investigated. The apparent activation energy of R_{CGO} was found to be 0.7–0.9 eV which is slightly lower compared with results obtained at 0.2 bar. The results obtained from fitting at low oxygen partial pressures are affected by the mass transport processes, which may therefore decrease the apparent activation energy.

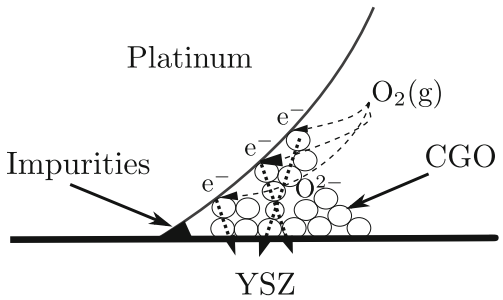

Fig. 9 Sketch of the interface between a platinum and YSZ grain with impurities blocking the TPB and with CGO grains forming an ionically conducting pathway

The polarisation resistance was found to decrease with increasing annealing temperature and increasing CGO grain size. The results were obtained from impregnated electrodes with a high loading and high coverage on the surface of the platinum grains for which the CGO phase facilitate transport of oxide ions, as mentioned above. The polarisation may therefore decrease if the conductivity of oxide ions in the CGO phase is increased. Previous investigations have shown that the oxygen ion conductivity of nano-sized CGO grains increases with decreasing grain size [3]. However, these results were obtained from measurements on dense samples. The CGO phase obtained from impregnation is porous as shown in Figs. 1 and 2. By increasing the annealing temperature, the CGO layer becomes more dense, which may therefore enhance the oxygen ion conductivity thereby decreasing the polarisation resistance, as mentioned above. However, there was no correlation between R_{CGO} and the annealing temperature. The impurities also become more mobile at higher temperature which enhances the segregation on the CGO grains. This could increase the effective TPB length at the Pt/YSZ interface, thereby decreasing the polarisation resistance.

For the impregnated electrodes annealed at various temperatures the CGO loading varies between 0.34 and 0.74 mg cm^{-2}. However, there was no correlation between the polarisation resistance and the CGO loading above around 0.4 mg cm^{-2} as mentioned above and the electrodes 4.2 to 4.9 were impregnated following the same approach. The loading of CGO should therefore not influence the observed tendency. The results showed that CGO decreased the polarisation resistance related to the oxygen reaction, which dominated the impedance at temperatures below 496 °C, and at low oxygen partial pressures, around 5×10^{-5} bar. At similar oxygen partial pressures between 596 and 744 °C, a temperature-independent process, related to mass transport by gas diffusion and convection, dominated the impedance. Impregnation with CGO did not affect this process significantly. The results obtained by Gur et al. [32] using cyclic voltammetry, also showed that a temperature-independent process became rate determining at low oxygen partial pressures and high temperatures.

Conclusion

The polarisation resistance of porous platinum electrodes was decreased by up to an order of magnitude by

impregnation with CGO. For high loadings, a porous layer of CGO was formed on the surface of the platinum grains, which facilitated transport of oxide ions thereby increasing the effective TPB length. Above a CGO loading of 0.4 mg/cm [2], there was no correlation between the polarisation resistance and the CGO loading. The polarisation resistance of the CGO impregnated electrodes was found to decrease with increasing annealing temperature which is interpreted as due to an increased oxide ion conductivity of the CGO phase. The increased TPB length would make the platinum electrode more robust and tolerant to poisoning. CGO was found to decrease the apparent activation energy of the oxygen reaction at an oxygen partial pressure of 0.2 bar and increase it at an oxygen partial pressure of 5×10^{-5} bar. Gas phase mass transport processes became dominating above 600 °C at an oxygen partial pressure of 10^{-5} bar. The addition of CGO did not have any significant effect on the mass transport processes.

Acknowledgements This work was supported financially by The Programme Commission on Sustainable Energy and Environment, The Danish Council for Strategic Research, via the Strategic Electrochemistry Research Center (SERC) (www.serc.dk), contract no. 2104-06-0011.

References

1. Mogensen M, Sammes N, Tompsett G (2000) Solid State Ionics 129:63–94
2. Steele BCH (2000) Solid State Ionics 129:95–110
3. Suzuki T, Kosacki I, Anderson HU (2002) J Am Ceram Soc 85:1492–1498
4. Trovarelli A (2002) Catalysis by ceria and related materials. World Scientific, UK
5. Patil KC, Hegde MS, Rattan T, Aruna ST (2008) Chemistry of nanocrystalline oxide materials: combustion synthesis, properties and applications. World Scientific, UK
6. Blennow P, Hansen K, Wallenberg L, Mogensen M (2007) J Eur Ceram Soc 27:3609–3612
7. Jiang SP, Chen XJ, Chan SH, Kwok JT (2006) J Electrochem Soc 153:A850
8. Chen X, Liu Q, Chan S, Brandon N, Khor K (2007) Electrochem Commun 9:767–772
9. Barbucci A, Bozzo R, Cerisola G (2002) Electrochim Acta 47:2183–2188
10. Badwal SPS, Bannister MJ, Ciacchi FT, Hooshmand GA (1988) J Appl Electrochem 18:608–613
11. Velle OJ, Norby T (1992) Solid State Ionics 52:93–97
12. Shuk P, Bailey E, Guth U (2008) Sensors (Peterborough, NH) 90:174–184
13. Lee JH (2003) J Mater Sci 38:4247–4257
14. Moos R (2005) Int J Appl Ceram Technol 2:401–413
15. Stetter JR, Li J (2008) Chem Rev (Washington, DC, U S) 108:352–366
16. Arakawa T, Saito A, Shiokawa J (1982) Bull Chem Soc Jpn 55:2273–2274
17. Rupp JL, Infortuna A, Gauckler LJ (2006) Acta Mater 54:1721–1730
18. Brauer G, Gradinger H (1954) Z Anorg Allg Chem 276:209–226
19. Orazem ME, Tribollet B (2008) Electrochemical impedance spectroscopy. Wiley, New Jersey
20. Opitz AK, Fleig J (2010) Solid State Ionics 181:684–693
21. Mitterdorfer A, Gauckler L (1999) Solid State Ionics 117:187–202
22. Boukamp BA, Bouwmeester HJM (2003) Solid State Ionics 157:29–33
23. Hitz C, Lasia A (2001) J Electroanal Chem 500:213–222
24. Badwal SPS (1984) J Mater Sci 19:1767–1776
25. Levy C, Guizard C, Julbe A (2007) J Am Ceram Soc 90:942–949
26. Primdahl S, Mogensen M (1999) J Electrochem Soc 146:2827
27. Jacobsen T, Hendriksen P, Koch S (2008) Electrochim Acta 53:7500–7508
28. Primdahl S, Mogensen M (1998) J Electrochem Soc 145:2431
29. Bernasik A (2002) J Phys Chem Solids 63:233–239
30. Hughes AE, Badwal SPS (1991) Solid State Ionics 46:265–274
31. Hertz JL, Rothschild A, Tuller HL (2008) J Electroceram 22:428–435
32. Gur TM, Raistrick ID, Huggins RA (1980) J Electrochem Soc 127:2620